Computer-aided diabetic retinopathy diagnostic model using optimal thresholding merged with neural network

Ambaji S. Jadhav
Department of Electrical and Electronics,
B.L.D.E.A's V.P. Dr. P.G. Halakatti College of Engineering and Technology
(Affiliated to Visvesvaraya Technological University), Vijayapur, India

Pushpa B. Patil
Department of Computer Science and Engineering,
B.L.D.E.A's V.P. Dr. P.G. Halakatti College of Engineering and Technology
(Affiliated to Visvesvaraya Technological University),
Vijayapur, India, and

Sunil Biradar
Department of Ophthalmology,
Shri B. M. Patil Medical College and Research Center (Deemed to be University),
Vijayapur, India

Abstract

Purpose – Diabetic retinopathy (DR) is a central root of blindness all over the world. Though DR is tough to diagnose in starting stages, and the detection procedure might be time-consuming even for qualified experts. Nowadays, intelligent disease detection techniques are extremely acceptable for progress analysis and recognition of various diseases. Therefore, a computer-aided diagnosis scheme based on intelligent learning approaches is intended to propose for diagnosing DR effectively using a benchmark dataset.

Design/methodology/approach – The proposed DR diagnostic procedure involves four main steps: (1) image pre-processing, (2) blood vessel segmentation, (3) feature extraction, and (4) classification. Initially, the retinal fundus image is taken for pre-processing with the help of Contrast Limited Adaptive Histogram Equalization (CLAHE) and average filter. In the next step, the blood vessel segmentation is carried out using a segmentation process with optimized gray-level thresholding. Once the blood vessels are extracted, feature extraction is done, using Local Binary Pattern (LBP), Texture Energy Measurement (TEM based on Laws of Texture Energy), and two entropy computations – Shanon's entropy, and Kapur's entropy. These collected features are subjected to a classifier called Neural Network (NN) with an optimized training algorithm. Both the gray-level thresholding and NN is enhanced by the Modified Levy Updated-Dragonfly Algorithm (MLU-DA), which operates to maximize the segmentation accuracy and to reduce the error difference between the predicted and actual outcomes of the NN. Finally, this classification error can correctly prove the efficiency of the proposed DR detection model.

Findings – The overall accuracy of the proposed MLU-DA was 16.6% superior to conventional classifiers, and the precision of the developed MLU-DA was 22% better than LM-NN, 16.6% better than PSO-NN, GWO-NN, and DA-NN. Finally, it is concluded that the implemented MLU-DA outperformed state-of-the-art algorithms in detecting DR.

Originality/value – This paper adopts the latest optimization algorithm called MLU-DA-Neural Network with optimal gray-level thresholding for detecting diabetic retinopathy disease. This is the first work utilizes MLU-DA-based Neural Network for computer-aided Diabetic Retinopathy diagnosis.

Keywords Diabetic retinopathy detection, Gray-level thresholding, Optimal trained neural network, Dragon fly algorithm, Levy update, Performance metrics

Paper type Research paper

1. Introduction

In the present health care world, medical imaging has emerged as a fundamental tool for storing the patent's records in the way of visual documentation, which helps to extract diverse information about various diseases. In general, diabetic retinopathy (DR), macular degeneration, hemorrhages, hypertension, neovascularization, vein occlusion, and glaucoma are a few kinds of retinal infections. In this criterion, the processing of optic disc as well as retinal blood vessels is the major indicators for checking the harshness of the above-mentioned retinal diseases (ElahehImani *et al.*, 2015). Mostly, DR disease impacts the retinal blood vessels of diabetic patients. All over the world, 347 million diabetic patients are suffering from DR, as stated by WHO (Shanthi and Sabeenian, 2019). Especially in the USA, more than 40% of 29.1 million diabetic patients are suffering from various phases of DR.

Since symptoms cannot build up until the disease turns into the stern, initial discovery via regular screening of DR is essential. In the entire world, digital fundal photography-based monitoring schemes are utilized to deal with the DR. Still, the cost-factor is screen lighted in these monitoring phases for the large population (Faust *et al.*, 2012). As the screening practices are extremely dependent on manual detection, it consumes more time for each case. To maintain the diagnosing process over a large population, the research investigation has concentrated on recognizing the strategies to detect DR automatically (Nazir *et al.*, 2019).

A fast diagnosis is the fundamental task to reduce the severity of the disease, and thus averting the occurrence of blindness. Many image analysis algorithms have been introduced to reduce the workload of human efforts, streamline retinal pathology monitoring from the last few decades (Quellec *et al.*, 2017). For classification, and detection of DR, several CAD-based techniques were utilized in the literature. The computer-based approaches notice the differences in normal and affected eye images, and further, utilize the differences to frame feature space. The collaboration of those features specifies the exact recognition of DR. This motivates the researchers in selecting fundus image evaluation for DR detection (Salamat *et al.*, 2019; Niemeijer *et al.*, 2009; Akram *et al.*, 2013; Quellec *et al.*, 2011). Various methods based on mathematical morphology (Sopharak *et al.*, 2008; Hassan *et al.*, 2015), NN (Zhang *et al.*, 2019; Liu *et al.*, 2019), pattern recognition (Galshetwar *et al.*, 2017), region growing approaches (Panda *et al.*, 2016), fuzzy C-means clustering (Kar and Maity, 2016), Gabor filter (Farokhian *et al.*, 2017) banks are present in the literature. Moreover, this research area still requires enhancement like complexity reduction of the method utilized and high accuracy attainment in detection.

The major contributions of this paper are shown below:

(1) The proposed algorithm termed as MLU-DA helps to improve the segmentation as well as the classification process, where the levels of thresholding are optimized by MLU-DA. Moreover, the same algorithm is utilized for accomplishing the training in NN. With this improvement, it is indented to maximize the segmentation accuracy, and minimize the classification error.

(2) The developed MLU-DA model on both segmentation and classification is very robust and reliable to improve the DR diagnostic system, which correctly assigning the labels to retinal fundus images as normal and DR affected images with high accuracy.

The arrangement of this paper is depicted as follows: Literature review and the features and challenges of existing methods are shown in Section 2. Section 3 specifies the contribution of the proposed DR detection model. Section 4 describes the steps utilized for the DR detection system. Results and discussions are specified in Section 5. Finally, the conclusion of this paper is described in Section 6.

2. Literature review

2.1 Related works

Chakraborty et al. (2019) have implemented a supervised learning method by ANN to acquire high precise diagnoses outputs regarding DR detection. The extractions of features from retinal images are given as inputs to a well-performing detection algorithm called ANN. By guessing many entities of the conventional ANN, ANN architecture was personalized, which were adopted to enhance the accuracy. In the proposed method, the back propagation-based NN was used. From the results, the accuracy acquired by the introduced approach was 97.13%, which in turn confirmed that the suggested method was used to identify DR efficiently in the future.

Sangeetha and Maheswari (2018) have suggested the retinal image segmentation and blood vessels elimination via edge detection, thresholding, adaptive histogram equalization and morphological processing. From the fundus image, to find the automatic diagnosis of DR, a network with the CNN was introduced for exactly categorizing its seriousness. Here, the images gathered from Aravind Eye Hospital, and the widely accessible datasets like DIARETDB0, DIARETDB1_v1, and DRIVE, were trained using High-end GPU. Hence, the results obtained an accuracy of 96.9%, the specificity of 93%, and a sensitivity of 98% for the database containing 854 images.

Zhou et al. (2018) have recommended a MIL approach for DR detection, in which the classifiers and features were learned together from data to attain an effective enhancement on recognizing the lesions present inside. Specially, a pre-trained CNN was modified to accomplish the patch-level DR evaluation, and further, the global aggregation was considered for the DR image categorization. For DR detection of images, the results have attained a region under the ROC curve of 0.960 on Messidor and 0.925 on other datasets from Kaggle. To identify the DR lesions, the sensitivity of 0.995, the precision of 0.863, and an F_1-score of 0.924 on DIARETDB1 were attained by the linked component level proof.

Wan et al. (2018) have proposed CNNs-based DR detection to find an automated way to categorize a known group of fundus images. The suggested method consisted of three main complicated challenges like classification, segmentation, and detection. Here, VggNet, GoogleNet, ResNet and AlexNet were taken to analyze the performance of the DR classification by linking hyper-parameter tuning and transfer learning. Openly obtainable Kaggle platform was utilized to train these models. Finally, the results have attained the best classification accuracy of 95.68%, and the outputs have verified that the transfer learning and CNN mechanisms were showing improved accuracy on DR image classification.

Hemanth et al. (2019) have employed a mechanism, which consists of service of image processing by CLAHE, and the histogram equalization approaches. Later, the detection of DR was implemented by the classification of CNN. The approach was evaluated on the Messidor database that consists of 400 retinal fundus images, and from the experimental results, the accuracy of 97%, was achieved. Moreover to those results, a common assessment of formerly accomplished results has specified that the developed approach was effective and vigorous for detecting DR from retinal fundus images. By making use of the significant deep learning methods and image processing methods for detecting DR, the introduced technique and the outcomes achieved were noted as beneficial contributions to the identified research.

Li et al. (2019) have offered a sequence of deep-learning-based algorithms for monitoring DR automatically for attaining maximum specificity and sensitivity. Though, the deep learning methods did not execute well in clinical applications because of the restrictions of the state-of-the-art openly existing fundus images datasets. For validating these approaches in clinical circumstances, from 9,598 patients 13,673 fundus images were gathered and that images were split by seven graders into six classes based on DR level and quality of the image. In order to define four kinds of DR-related lesions, 757 DR images were preferred. At last, existing deep learning algorithms on gathered images were evaluated, with three main

detection procedures. Though the accuracy of 0.8284 was attained for DR recognition, these methods execute the poor, thus concludes that lesion detection and segmentation are complex. At last, a new dataset was provided named DDR for reviewing deep learning methods in clinical applications, especially for lesion identification.

Zeng et al. (2019) have recommended a model named computer-aided diagnosis that is depending on the deep learning algorithms for detecting RDR automatically by categorizing color retinal images into two grades. A novel CNN by Siamese like structure was trained with a mechanism known as transfer learning. The introduced models recognized the binocular fundus images as inputs and study the relationship to assist in prediction when compared to the earlier works. By using the binocular model, the AUC of 0.951 was achieved with the training set of 28,104 images and a test set of 7,024 images, which was 0.11 better than the conventional monocular approach. To check the efficiency of binocular design, five class DR detection was trained and assessed on a 10% validation set. Hence, the result represents that it attains a kappa score of 0.829, which was better when compared to the existing non-ensemble approach. Hence, the result represents that it attains a kappa score of 0.829, which was better when collated over the existing non-ensemble approach.

Ramos et al. (2018) have introduced an approach to decrease the noise of the RGB image present in the green channel with Low-pass Radius Filter. Next, a Gaussian fractional derivative and a 30-element Gabor filter were utilized for extremely improving the shape and structure of the blood vessels. After that, a sequence of morphology-based regulations and threshold was utilized to decrease the occurrence of false-positive pixels and segregate the blood vessels. Also, the proposed approach was for detecting and removing the optic disc from the image. For DRIVE dataset, the suggested approach has attained a specificity of 0.7854, and an accuracy of 0.9503. The performance validation was carried out over existing approaches like the Adaptive threshold, multiple classes Otsu technique, and the threshold for a Frangi filter. Next to the evaluation under computer simulations, it was accomplished that the recommended approach was aggressive and consistent for the blood vessel segmentation.

Sun and Zhang (2019) have proposed Electronic Health Records (EHR) which gradually become an effective measure to prevent DR disease. The machine learning models are used to diagnose the DR in patients with the EHR data and formed a set of treatment methods. It can predict the patient samples. The data and features are used to determine the limit of machine learning, models and algorithms. The most important characteristics are the influence of binding the unsaturated iron, which was the index of protein synthesis in blood.

Hua et al. (2019) have introduced a bimodal learning approach using a Trilogy of Skip-connection Deep Networks (Tri-SDN) for DR risk progression prediction. It is used for acquiring DR-oriented knowledge through conventional machine learning techniques, which require the most impactful risk factors. It lowers the necessity of constructing and training the designated deep learning model with a large-scale dataset of fundus photography.

2.2 Review
Numerous researches have given attention to finding the alternative form of actions to diagnose the DR in an automated manner, yet, there are various questions, and challenges need to be resolute in the future. A few of the major pros and cons are represented in Table 1. ANN (Chakraborty et al., 2019) is simplified, after learning from the early inputs and their relationships, it can assume unseen relationships on hidden data as well, and can learn and model nonlinear and complex relationships. Still, there are some conflicts like there are no particular restrictions to determine the structure of ANN, appropriate network structure will acquire through experience and trial and error, and can work only with numerical data, before establishing to ANN, the problems need to be translated into numerical values. CNN (Sangeetha and Maheswari, 2018; Zeng et al., 2019) has high accuracy in recognizing image

Authors [Citations]	Methodology	Features		Challenges	
Chakraborty et al. (2019)	ANN	(1)	Has the capacity to learn and model non-linear and complex relationships	(1)	There are no particular restrictions to determine the structure of ANN, an appropriate network structure will acquire through experience and trial and error
		(2)	ANNs are simplified, after learning from the early inputs and their relationships; it can assume unseen relationships on hidden data as well	(2)	ANNs can work only with numerical data. Before establishing to ANN, the problems need to be translated into numerical values
Sangeetha and Maheswari (2018)	CNN	(1)	High accuracy in recognition of image problems	(1)	It requires a large dataset
		(2)	To extract significant data at a low computational cost	(2)	It is dependent on hardware
Zhou et al. (2018)	MIL	(1)	It has high accuracy	(1)	Requires additional image quality evaluation
		(2)	It provides more information than learning by single instance representation		
Wan et al.(2018)	Deep CNN	(1)	It has high accuracy	(1)	They are slow to train if the GPU was not good
		(2)	It does not require feature extraction		
Hemanth et al. (2019)	Deep CNN	(1)	They are flexible and work well on image-related data	(1)	It is still using the black box technique
		(2)	Features are not pre-trained		
Li et al. (2019)	Deep learning	(1)	Has the capacity to execute feature learning by own	(1)	It is highly expensive to train because of the complex data
		(2)	It is highly efficient at delivering good quality results	(2)	It requires a large amount of processing power
Zeng et al. (2019)	CNN	(1)	It provides a fast diagnosis	(1)	It is computationally high cost
		(2)	It automatically detects the main features without any human guidance		
Ramos et al. (2018)	Thresholding Classification	(1)	It does not require prior information about the image	(1)	Specificity and sensitivity need to be improved
		(2)	It is fast and easy to implement		
Sun and Zhang (2019)	EHR	(1)	It can transform a large number of unstructured	(1)	It temporarily loses the productivity associated with privacy and security concerns
		(2)	irregular and noisy feature data		
Hua et al. (2019)	Tri-SDN	(1)	It can reduce the dependence to determine strong effects on the progression of DR	(1)	Fundus images need to be improved

Table 1.
Features and challenges of conventional diabetic retinopathy detection models

problems to extract significant data at low computational cost, as well as it provides fast diagnosis, and automatically detects the main features without any human guidance. But, there are some challenges such as it requires large dataset, computationally high cost, and it is dependent on hardware. MIL (Zhou *et al.*, 2018) has high accuracy, provides more information than learning by single instance representation. Though, it requires additional image quality evaluation. Deep CNN (Wan *et al.*, 2018; Hemanth *et al.*, 2019) has high accuracy; moreover, it does not require feature extraction, they are flexible and work well on image-related data, and features do not require pre-training. Yet, there are some disadvantages like they are slow to train if the GPU was not good, and it is still using the black-box approach. Deep learning (Li *et al.*, 2019) can execute feature learning on their own, and it is highly efficient at delivering good quality results. But, it is highly expensive to train because of the complex data, and it requires a large amount of processing power. Threshold classification (Aguirre-Ramos *et al.*, 2018) does not require prior information of the image, and it is fast and easy to implement. However, it is having few defects like specificity and sensitivity need to be improved. Therefore, some challenges need to be determined in the future by considering the above-mentioned constraints. Therefore, above-revealed challenges are extremely encouraged to enhance future researches.

3. Contribution of proposed diabetic retinopathy detection model

3.1 Archetype of proposed model

The proposed architecture of DR detection is given by Figure 1. This model introduces an automatic DR detection system capable of differentiating the normal and abnormal (DR affected) images of different retinal fundus images, which are commonly utilized for detecting the eye-related diseases via image processing technology. The proposed model involves four main phases: (1) image pre-processing, (2) blood vessel segmentation, (3) feature extraction, and (4) classification. In the pre-processing phase, the retinal fundus images are subjected to two processes like CLAHE and average filtering. Here, the CLAHE technique is applied for enhancing the local contrast of the image, and the average filtering is applied later to remove the noise from the image, which in turn helps to preserve the sharp features. After pre-processing, the blood vessel segmentation is done based on a few steps. At first, the contrast-enhanced images, and the filtered images are thresholded using gray-level thresholding. Further, SIFT is used to extract the key points K_1 and K_2 of the contrast-enhanced images and the filtered images, respectively. The two images with key points K_1 and K_2 are subtracted and further applied for gray-level thresholding. Both the enhanced and the keypoints extracted images are added, and the final blood vessel segmented image is obtained. Once the blood vessels are segmented, the feature extraction procedure is done to extract the features. Here, three types of features are intended to extract namely, (1) LBP, (2) TEM, and (3) Entropy. LBP is performed to strengthen the performance effectively, TEM is used to find the energy present in the region filters, and entropy is calculated by two metrics known as Shannon and Kapur. All these features are combined and applied to the NN-based classifier for classifying either normal or abnormal images.

The novelty of the architectural model relies on two phases:

(1) Segmentation: For the gray-level-based segmentation process, the levels of thresholding are optimized using the proposed MLU-DA to maximize the accuracy among the ground truth and segmented images.

(2) Classification: The training algorithm LM is replaced by proposed MLU-DA, which updates the weights of NN for reducing the classifier error.

Let S be the input image considered for DR detection, S_{CLAHE} be the CLAHE-based contrast-enhanced image, S_{filt} be the average filtered image, S_{seg} be the blood vessel segmented image,
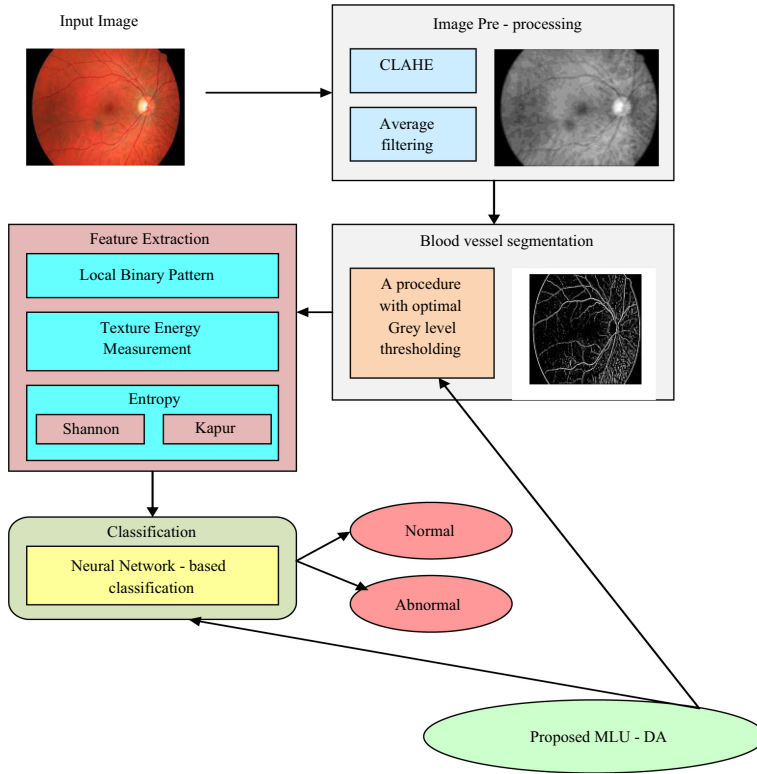
and FE_e be the entire features extracted from the segmented blood vessels, where $e = 1, 2, \cdots N_F$, and N_F be the number of features.

3.2 Objective model
The objective model of the current DR detection model is focused on two areas. One is segmentation, and the other is classification.

(1) Maximizing the accuracy of segmentation: The initial objective function is the maximization of accuracy between the segmented blood vessels and the ground truth image. The initial objective function in the segmentation phase is shown in Eq. (1), where A refers to accuracy.

The formulation for computing the accuracy is given in Eq. (2), where PA^T denotes true positive of the elements, PA^F denotes true negative, FA^T indicates false positive, and FA^F indicates the false negative.

$$\mathrm{Obj1} = \mathrm{Max}(A) \tag{1}$$

$$A = \frac{\mathrm{PA}^T + \mathrm{PA}^F}{\mathrm{PA}^T + \mathrm{PA}^F + \mathrm{FA}^T + \mathrm{FA}^F} \tag{2}$$

(2) Minimizing the detection error: The second objective considers the minimization of error difference between the detected and actual outcomes. The objective function of the NN is denoted in Eq. (3), where ME is the error function specified in Eq. (32).

$$\text{Obj2} = \text{Min(ME)} \tag{3}$$

3.3 Solution encoding

The solution encoding of the segmentation and classification by the proposed MLU-DA is shown in Figure 2. In gray-level thresholding-based segmentation, the levels of thresholding are optimized by proposed MLU-DA, where L is the level, in which the maximum and the minimum bounding limit is in the range $[-20, 20]$. In the classification phase, the weights are updated in the NN by the same proposed MLU-DA, where N_B denotes the total number of weights in different layers of NN.

3.4 Conventional dragonfly optimization algorithm

The segmentation and classification phases of the proposed DR detection model is improved by the modified DA. The main inspiration of DA (Jafari and Chaleshtari, 2017) is based on the behavior of swarms, which is either static or dynamic. The entities of a swarm must strive for the food and divert the enemies. Based on Jafari and Chaleshtari (2017), there are five key factors to be considered for updating the location of the individuals in swarms. "Cohesion, alignment, separation, attraction and distraction" are the main factors of the behaviors of the dragonflies. The separation of cth dragonfly, Se_c build its neighbors as shown in Eq. (4), where X be the location of the present individual, X_d denotes the location of dth neighboring individual and N be the count of neighboring individuals. Next, alignment is computed using Eq. (5), where Ve_d be the velocity of dth neighboring individual. Similarly, control cohesion is determined as represented in Eq. (6). Later, the attraction in the direction of food is evaluated as shown in Eq. (7), where Food refers to the location of the source of food. Finally, the distraction towards the enemy is computed as per Eq. (8), where Enemy specifies the position of the enemy.
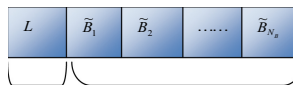
$$Se_c = -\sum_{d=1}^{N}(X - X_d) \tag{4}$$

$$Al_c = \frac{\sum_{d=1}^{N} Ve_d}{N} \tag{5}$$

$$Co_c = \frac{\sum_{d=1}^{N} X_d}{N} - X \tag{6}$$

$$AF_c = \text{Food} - X \tag{7}$$

$$DE_c = \text{Enemy} + X \tag{8}$$

Figure 2.
Solution encoding of segmentation and classification

The terms like step (ΔX) and position (X) are the two vectors need to be considered for updating the positions of dragonflies. DA has introduced based on the inspiration flowed in the PSO algorithm (Pedersen and Chipperfield, 2010). Moreover, each dragonflies' act of moving is determined by step vector, which is computed based on Eq. (9), where it specifies the current iteration, se represents the separation weight, Se_c denotes the separation of cth individual, al indicates the alignment weight, Al_c is the alignment of cth individual, co specifies the weight of cohesion, Co_c indicates the cohesion of cth individual, af be the food factor, AF_c denotes the food source of cth dragonfly, de be the enemy factor, DE_c indicates the location of an enemy of the cth individual, and δ be the weight of inertia. The position vector is computed as shown in Eq. (10).

$$\Delta X_{it+1} = (seSe_c + alAl_c + coCo_c + af\,AF_c + deDE_c) + \delta \bullet \Delta X_{it} \tag{9}$$

$$X_{it+1} = X_{it} + \Delta X_{it+1} \tag{10}$$

If there is no neighboring solution, the dragonfly has to fly around the search space via a random walk by rising the randomness, and stochastic characteristics and exploration. At this point, the dragonflies are updated as shown in Eq. (11), Eq. (12), Eq. (13), and Eq. (14) where dpv is the position vector, rn_1 and rn_2 are the random numbers ranging between [0, 1], and ξ is the constant.

$$X_{it+1} = X_{it} + \text{Levy}(dpv) \times X_{it} \tag{11}$$

$$\text{Levy}(dpv) = 0.01 \times \frac{rn_1 \times \phi}{|rn_2|^{\frac{1}{dpv}}} \tag{12}$$

$$\phi = \left(\frac{\Gamma(1+\xi) \times \sin\left(\frac{\Pi\xi}{2}\right)}{\Gamma\left(\frac{1+\xi}{2}\right) \times \xi \times 2^{\left(\frac{\xi-1}{2}\right)}} \right)^{\frac{1}{\xi}} \tag{13}$$

$$\Gamma(w) = (w-1)! \tag{14}$$

Moreover, Eq. (9) defines the step vector, and Eq. (10) defines the updated position of the dragonfly. The neighborhood of an individual dragonfly is established by computing the Euclidean distance among all the dragonflies, and further updates X and ΔX. The algorithmic representation of conventional DA is shown in Algorithm 1.

Algorithm 1: Pseudocode of existing DA (Jafari & Chaleshtari, 2017)
The entire solutions of dragonflies X is initialized
The step vectors ΔX are initialized
while the final condition is not satisfied
Update source of food & enemy
update δ, se, al, co, af, and de
Compute Se, Al, Co, AF, and DE
Update the radius of neighbours
If a dragonfly has atleast one neighbouring dragonfly
Eq. (10) is used to update velocity vector
Eq. (11) is used to update position vector
Else
Eq. (12) is used to update position vector
end if
Validate the updated solution by fitness evaluation
end while

3.5 Proposed MLU-DA

Rather than the beneficial part of conventional DA, it still faces some critical drawbacks like premature convergence, and unbalanced exploration, and exploitation. To improve the performance of existing DA to a particular extent, and develop an effective method to improve the segmentation and classification for DR detection, the modified algorithm called MLU-DA is implemented here. The advantages of MLU-DA include, high accuracy, remarkable stability, increasing population diversity, accelerating the convergence, strong robustness, powerful optimizing ability, and higher precision. As a modification, the levy-based update in Eq. (11) will be replaced by a new formula, which is given in Eq. (15).

$$X_{it+1} = we \times X_{it} + af(\text{Food} - X_{it+1}) \tag{15}$$

Here, *we* refers to the weight function. This new update helps to provide better convergence to the proposed MLU-DA. The pseudo-code of the proposed MLU-DA is shown in Algorithm 2.

Algorithm 2: Pseudocode of proposed MLU-DA
The entire solutions of dragonflies X is initialized
The step vectors ΔX are initialized
while the final condition is not satisfied
Update source of food & enemy
update δ, se, al,
co, af, and de
Compute Se, Al, Co, AF, and DE
Update the radius of neighbours
If a dragonfly has atleast one neighbouring dragonfly
Eq. (10) is used to update velocity vector
Eq. (11) is used to update position vector
Else
Update position vector based on new levy-based formulation using Eq. (15).
end if
Validate the updated solution by fitness evaluation
end while

4. Steps utilized for diabetic retinopathy detection system

4.1 Image pre-processing

Here, image pre-processing of retinal fundus image is done using (1) CLAHE and (2) gray-level thresholding.

(1) *CLAHE*: It provides the optimal equalization regarding maximum entropy and restricts the brightness of the image. This approach is used for enhancing the contrast of the images. Implementation of CLAHE is as follows: (1) Split every input image into non-overlapping contextual regions of the same size containing 8×8 blocks, each correlates to the neighborhood of 64 pixels. (2) The intensity histogram of every contextual region is to be computed. (3) Set the clip limits for clipping the histograms. It is the threshold parameter to adapt the brightness of the image efficiently. It needs to be set to the minimum optimal value. (4) By choosing the transformation functions, each histogram is changed. (5) Every histogram is modified using the limit of the fixed clip limit. The numerical representation is given in Eq. (16), where a denotes the calculated pixel value, $a_{\max}$ be the maximum pixel value, $a_{\min}$ be the minimum pixel value, and $CP(b)$ denotes the cumulative probability distribution. For exponential distribution, the gray level is modified as Eq. (17), where α indicates the clip parameter. CLAHE technique works on small portions of the image known as "tiles" instead of the whole image. The brightness of every tile is improved so that the output region of the histogram rough matches the histogram mentioned by the distribution type. (6) The neighboring tiles are united by bilinear interpolation, and the grayscale values of

the image are changed corresponding to the improved histograms.

$$a = [a_{max} - a_{min}]*CP(b) + a_{min} \qquad (16)$$

$$a = a_{min} - \left(\frac{1}{\alpha}\right)*\ln[1 - CP(b)] \qquad (17)$$

After applying CLAHE, the image S_{CLAHE} is obtained, which is further given for filtering using the average filter.

(2) *Average filtering*: It is used to improve the template on the target pixel, and further takes the average of entire pixel values. The feature of the image helps to observe the size and shape of the image. Let the size of the template be $m_s \times m_t$, where m is odd. The representation of average filtering for the image S_{CLAHE} is based on Eq. (18).

$$S_{filt} = \frac{1}{M}\sum S_{CLAHE}(i,j) \qquad (18)$$

4.2 Procedure for blood vessel segmentation
Once the pre-processing is completed, the image is moved forward to the blood vessel segmentation process. The current blood vessel segmentation procedure is depending on the following steps.

(1) Take two pre-processed images S_{CLAHE} and S_{filt}. Apply SIFT operation (Sreedharan *et al.*, 2018) to both S_{CLAHE} and S_{filt} obtain two images with its key points. Further, find the difference between the images with two sets of keypoints followed by optimized gray-level thresholding and apply a morphological operation called area opening to eliminate the small pixels.

(2) Directly apply subtraction operation on S_{CLAHE} and S_{filt}, followed by optimized gray-level thresholding and morphological operation.

(3) Sum the two images for obtaining the final segmented image.

Gray-level thresholding: It is based on the global thresholding that is depending on the belief that the image has a bimodal histogram. Hence, an easy procedure can be exploited for extracting the object from the background. While performing this operation, the level of threshold L is used, this divides the modes. The thresholded image is given in Eq. (19) that results in a binary image, whereas the pixels with intensity value 1 is equivalent to objects and 0 is equivalent to the background.

$$S_{thresh} = \begin{cases} 1 & \text{if } S(x,y) > L \\ 0 & \text{if } S(x,y) \leq L \end{cases} \qquad (19)$$

The novelty of the proposed segmentation procedure is to optimize the threshold level L using MLU-DA, which results in attaining high segmentation accuracy. Hence, the segmented image S_{seg} is obtained.

4.3 Feature extraction
The feature extraction for the segmented blood vessels uses three approaches (1) LBP, (2) LTE and (3) Entropy.

(1) *LBP:* LBP is introduced as a strong and effective texture descriptor. Principally, it can be applicable to a broad range of various applications from texture segmentation to detection (Liao *et al.*, 2009). LBP operator labels the pixels of an image by thresholding the neighborhood of each pixel with the middle value, and the output of this thresholding is obtained in the form of the binary number. The histogram of the

labeled image $S_{\text{seg}}(x, y)$ is utilized as a descriptor and is defined in Eq. (20), where n denotes the number of labels given by LBP operator and $I(A) = 1$ when A is true, A is false when $I(A) = 0$.

$$Hg_{im} = \sum_{x,y} I(S_{\text{seg}}(x,y) = im), \; im = 0, \cdots, n-1 \tag{20}$$

To acquire a rotation-invariant uniform pattern using finger angular quantization, a uniformity measure (UM) is determined based on Eq. (21) by considering LBP$_{\text{PB,RB}}$ as a PB-bit binary number $(r_{\text{PB}-1}, r_{\text{PB}-2}, \cdots, r_1 r_0)$. The rotation invariant uniform pattern with UM value less than or equal to 2 is described in Eq. (21), where the term g_{pv} denotes the gray value of the center pixel, g_{cv} denotes the gray value of PB points, and $p = 0, \cdots, \text{PB} - 1$.

$$\text{UM}(\text{LBP}_{\text{PB,RB}}) = |r_{\text{PB}-1} - r_0| + \sum_{\text{PB}=1}^{\text{PB}-1} |r_{\text{PB}} - r_{\text{PB}-1}| \tag{21}$$

$$\text{LBP}_{\text{PB,RB}} = \left\{ \sum_{p=0}^{\text{PB}-1} S(g_{pv} - g_{cv}) \; \text{if} \; \text{UM}(\text{LBP}_{\text{PB,RB}}) \leq 2 \right. \tag{22}$$

With the help of LBP, by selecting circles with different radii around the center pixels, a multi-scale examination is performed and then creating a separate LBP image for every scale. Entropy and energy of the LBP image is built over the various count of pixels (PB = 8, 16, and 24, and RB = 1, 2 and 3 respectively) are utilized as feature descriptors.

(2). *LTE*: Law's mask (Gupta and Undrill, 1995) is considered as a well-performing texture descriptor, which has been utilized in different applications. It is based on the texture energy changes appealed to the image for evaluating the energy present in the pass region of filters [48]. Entire masks are obtained from the one-dimensional vector of five-pixel lengths $L5, E5, S5, R5, W5$, which referred to level, spot, edge, ripple, and wave, respectively.

Initially, the image is convoluted with a 2D mask for extracting the texture data from the segmented S_{seg} image. The obtained texture image is based on Eq. (23), if the filter $L5E5$ is used.

$$\text{Tex}_{L5E5} = S_{\text{seg}}(i,j) \otimes L5E5 \tag{23}$$

Based on laws, to filter $L5E5$ image $I(i,j)$ is represented in Eq. (19). All the two dimensional masks had zero mean except $L5L5$. Hence, the texture image Tex_{L5L5} is utilized to normalize the contrast of the remaining texture images $\text{Tex}(i,j)$, which is shown in Eq. (24). The outputs are transferred to TEM filters that include moving nonlinear window average of absolute values as described in Eq. (25). By merging 25 TEM descriptors, an invariant TEM (TR) is obtained and is shown in Eq. (26).

$$\text{Normalize}(\text{Tex}_{(i,j)}) = \frac{\text{Tex}_{(i,j)}}{\text{Tex}_{(i,j)^{L5L5}}} \tag{24}$$

$$\text{TEM}_{(i,j)} = \sum_{p=-7}^{7} \sum_{q=-7}^{7} |\text{Tex}_{(i+pj+q)}| \tag{25}$$

$$\text{TR}_{E5L5} = \frac{\text{TEM}_{E5L5} + \text{TEM}_{L5E5}}{2} \tag{26}$$

(3) *Entropy computation:* Entropy in general "defined as the uncertainty associated with the randomness. Here, two types of entropy measures are taken into consideration,

Shannon and Kapur entropy. Let $S_{\text{seg}}(x,y)$ be the segmented input image with N_{di} distinct gray value, whereas $(i = 0, 1, 2, \cdots, \text{LA} - 1)$. For a specified region of interest of size $(me \times ne)$, the normalized histogram is expressed based on Eq. (27).

$$En_{di} = \frac{N_{di}}{me \times ne} \tag{27}$$

Moreover, the computational formula for Shannon entropy is shown in Eq. (28). On the other hand, Kapur entropy has a more dynamic range than Shannon entropy over a range of broadcasting conditions, and it is used in evaluating regularity and scatter density. Kapur's entropy is described in Eq. (25), where α and β are the coefficients, and $\alpha \neq \beta$.

$$Sh = -\sum_{di=0}^{\text{LA}-1} En_{di} \log_2(En_{di}) \tag{28}$$

$$K_{\alpha,\beta} = \frac{1}{\beta - \alpha} \log_2 \frac{\sum\limits_{di=0}^{\text{LA}-1} En_{di}^{\alpha}}{\sum\limits_{di=0}^{L-1} En_{di}^{\beta}} \tag{29}$$

Hence, the combination of three features sets LBP, TEM, and entropy is represented as FE_e, where $e = 1, 2, \cdots N_F$, and N_F is the number of features.

4.4 Diabetic retinopathy detection

The feature sets FE_e is subjected to NN for categorizing the normal and abnormal images. NN (Fernández-Navarro *et al.*, 2017) is called a well-known scheme for classification in many applications owing to its flexibility. The advantages of Neural Network include, fast evaluation, easy to add and modify detection, can solve any machine learning problem, and can handle large number of features.

An improvement in training of NN is adopted here, which is diagrammatically shown in Figure 3.

Here, the input feature set is represented as FE_e, m is the input neuron, h is the hidden neuron, and *on* is the output neuron. In the NN architecture, the output of the hidden layer is computed based on Eq. (30), and the overall output of the network is represented in Eq. (31). Here, $IN(C)$ signifies the count of input neurons, $OP(C)$ refers to the count of hidden neurons, $\tilde{B}_{(\widehat{Wh})}^{(H)}$ describes the bias weight to hth hidden neurons, $\tilde{B}_{(\widehat{Won})}^{(O)}$ denotes the bias weight to *on*th output neuron, $\tilde{B}_{(mh)}^{(H)}$ shows the weight from mth input to hth hidden neurons, and $\tilde{B}_{(hon)}^{(O)}$ shows the weight from the hth hidden neuron to the *on*th output neuron. The term AC denotes the activation function, and the network output $\widehat{O}_{on}$ refers to the classified output.

$$\overline{H}^{(H)} = \text{AC}\left(\tilde{B}_{(\widehat{Wh})}^{(H)} + \sum_{m=1}^{IN(C)} \tilde{B}_{(mh)}^{(H)} FE_e\right) \tag{30}$$

$$\widehat{O}_{on} = \text{AC}\left(\tilde{B}_{(\widehat{Wn})}^{(O)} + \sum_{h=1}^{OP(C)} \tilde{B}_{(hon)}^{(O)} \overline{H}^{(H)}\right) \tag{31}$$

To provide better training to the NN, weight $B_z = \{\tilde{B}_{(\widehat{Wh})}^{(H)}, \tilde{B}_{(\widehat{Won})}^{(O)}, \tilde{B}_{(mh)}^{(H)}, \tilde{B}_{(hon)}^{(O)}\}$ is optimally selected by focusing on the objective function (minimum) as shown in Eq. (15), which is the
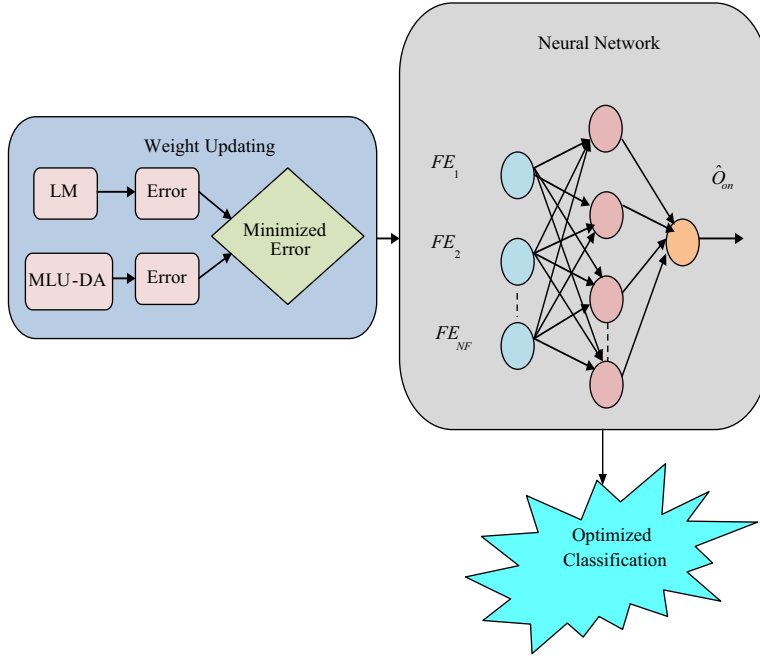
measured error.

$$\text{ME} = \underset{\left\{\tilde{B}_{(\widehat{Wh})}^{(H)}, \tilde{B}_{(\widehat{Won})}^{(O)}, \tilde{B}_{(mh)}^{(H)}, \tilde{B}_{(hon)}^{(O)}\right\}}{\text{argmin}} \sum_{on=1}^{O(C)} \left|O_{on} - \widehat{O}_{on}\right| \tag{32}$$

The error difference between the predicted amount $\widehat{O}_{on}$ and the actual amount O_{on} is given in Eq. (32), which should be minimized by optimizing the weight B_z using the proposed MLU-DA.

5. Results and discussions

5.1 Experimental setup
The developed DR diagnosis system was performed in MATLAB 2018a, and the simulation results was achieved. In this context, the evaluated standard dataset was taken from (https://www5.cs.fau.de/research/data/fundus-images/: Access date-2019-09-05-High Resolution Fundus (HRF) image datasets). For the experiment, the population size was considered as 50, and the count of iteration was fixed as 100. For segmentation analysis, the proposed MLU-DA-based gray-level thresholding was compared over PSO (Pedersen and Chipperfield, 2010), GWO (Mirjalili et al., 2014), WOA (Mirjalili and Lewis, 2016), and DA (Jafari and Chaleshtari, 2017)-based gray-level thresholding. On the other hand, the classification performance was analyzed with combined features (LBP + TEM + Entropy), and individual features as well. In addition, the performance of the optimally trained NN was contrasted with standard LM-NN (Fernández-Navarro et al., 2017).

5.2 Performance metrics
Here, ten performance metrics are considered for analyzing the performance. They are as follows:

(1) Accuracy: It is a "ratio of the observation of exactly predicted to the whole observations." The formula for accuracy is shown in Eq. (2).

(2) Sensitivity: It measures "the number of true positives, which are recognized exactly." It is mathematically represented in Eq. (33):

$$\text{Sensitivity} = \frac{\text{PA}^T}{\text{PA}^T + \text{FA}^F} \tag{33}$$

(3) Specificity: It measures "the number of true negatives, which are determined precisely." The specificity is formulated as Eq. (34):

$$\text{Specificity} = \frac{\text{PA}^F}{\text{FA}^T} \tag{34}$$

(4) Precision: It is "the ratio of positive observations that are predicted exactly to the total number of observations that are positively predicted." It is shown in Eq. (35):

$$\text{Precision} = \frac{\text{PA}^T}{\text{PA}^T + \text{FA}^T} \tag{35}$$

(5) FPR: It is computed as "the ratio of the count of false-positive predictions to the entire count of negative predictions." FPR is numerically represented in Eq. (36):

$$\text{FPR} = \frac{\text{FA}^T}{\text{FA}^T + \text{PA}^F} \tag{36}$$

(6) FNR: It is "the proportion of positives which yield negative test outcomes with the test." It is numerically denoted in Eq. (37):

$$\text{FNR} = \frac{\text{FA}^F}{\text{FA}^F + \text{PA}^T} \tag{37}$$

(7) NPV: It is the "probability that subjects with a negative screening test truly do not have the disease." It is represented in Eq. (38):

$$\text{NPV} = \frac{\text{FA}^F}{\text{FA}^F + \text{PA}^F} \tag{38}$$

(8) FDR: It is "the number of false positives in all of the rejected hypotheses." The formula for FDR is shown in Eq. (39):

$$\text{FDR} = \frac{\text{FA}^T}{\text{FA}^T + \text{PA}^T} \tag{39}$$

(9) F_1 score: It is defined as the "harmonic mean between precision and recall. It is used as a statistical measure to rate performance." It is numerically shown in Eq. (40):

$$F_1 \text{ score} = \frac{\text{Sensitivity} \bullet \text{Precision}}{\text{Precision} + \text{Sensitivity}} \tag{40}$$

(10) MCC: It is a "correlation coefficient computed by four values" as denoted in Eq. (41):

$$MCC = \frac{PA^T \times PA^F - FA^T \times FA^F}{\sqrt{(PA^T + FA^T)(PA^T + FA^F)(PA^F + FA^T)(PA^F + PA^F)}} \quad (41)$$

5.3 Analysis on segmentation

This section mainly concentrates on the segmentation analysis that is enhanced using gray-level thresholding. The developed MLU-DA-based gray-level thresholding was contrasted with existing PSO, GWO, WOA, and DA-based thresholding to evaluate the performance of the optimized segmentation. The outputs of the segmented images by the introduced MLU-DA based gray-level thresholding with the conventional PSO, GWO, WOA, and DA-based gray-level thresholding are shown in Figure 4, and the corresponding segmentation analysis is shown in Table 2. From Table 2, the accuracy of the proposed MLU-DA is 0.178% better than conventional gray-level thresholding, 0.183% better than PSO, 0.193% better than GWO and WOA, and 0.19% better than DA-based gray-level thresholding. The sensitivity of the developed MLU-DA algorithm is 13.9% superior to existing gray-level thresholding, 14.2% superior to PSO, 15% superior to GWO and WOA, and 14.6% superior to DA-based gray-level thresholding. Moreover, the precision of the implemented MLU-DA is 1.22% improved than state-of-the-art gray-level thresholding, 1.21% improved than PSO, 1.27% improved than GWO, and WOA, and 1.22% improved than DA-based gray-level thresholding. Similarly, the proposed segmentation shows the best performance for other performance metrics, which validates the effect of optimized thresholding on blood vessel segmentation. Therefore, it is confirmed that blood vessel segmentation performance by the implemented MLU-DA model is effective.

5.4 Texture feature analysis

This section specifies the analysis of texture features, which is the combination of LBP and TEM. The performance of the combined feature with MLUDA-NN is compared with the individual texture features as T-LM-NN, T-PSO-NN, T-GWO-NN, T-WOA-NN, T-DA-NN and MLUDA-NN. The performance analysis is graphically denoted in Figure 5, and the overall performance analysis of the texture features are shown in Table 3. From Figure 5 (a), the accuracy of the performance of the combined-MLUDA-NN is showing the best accuracy for exactly classifying the labels at the considered learning percentages as mentioned above. At a learning percentage of 90%, the implemented combined-MLUDA-NN system is 53.8% better than the T-DA-NN, 100% better than T-PSO-NN, and 62% better than T-MLUDA-NN. The sensitivity of Figure 5 (b) is showing its best performance overall learning percentages. Now, 50% learning percentage is considered and the performance of the developed combined-MLUDA-NN model is 8.88% improved than T-MLUDA-NN, and 15.2% improved than T-GWO-NN. In Figure 5 (c), the performance of specificity by the proposed combined-MLUDA-NN is better to precisely recognizing the true negative. It is 11.1% superior to T-MLUDA-NN, and 42.8% superior to T-PSO-NN when the learning percentage is taken as 70%. From Figure 5 (d), the precisions of all learning percentages are determined exactly with the positive observations. At a learning percentage of 90%, the precision of the combined-MLUDA-NN method is 66.6% enhanced than T-DA-NN, 100% enhanced than T-PSO-NN and T-MLUDA-NN, and 65% enhanced than T-GWO-NN. Similarly, the FPR and FDR of the developed combined-MLUDA-NN are seemed to be minimum at all learning percentages. At a learning percentage, 20%, the FNR of the suggested combined-MLUDA-NN model is 50% better than the T-MLUDA-NN and 66.6%
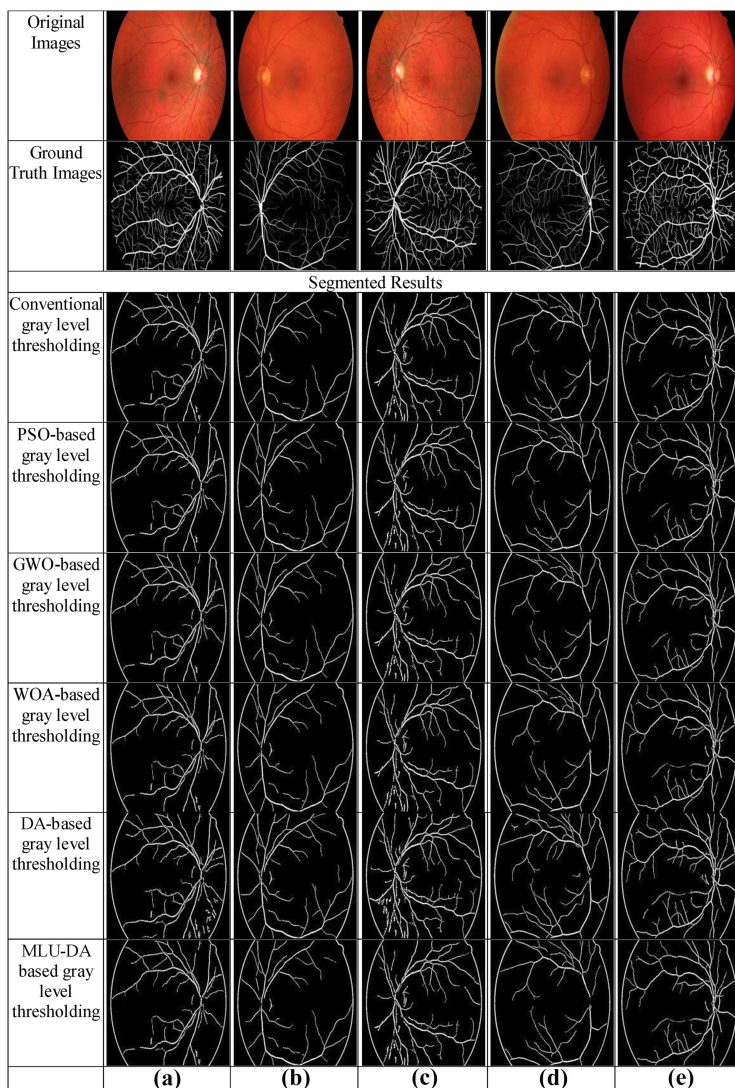
Figure 4.
Segmentation results
using proposed and
conventional
optimization algorithm
when gray-level
thresholding is taken
into consideration

better than T-GWO-NN, which is shown in Figure 5 (f). NPV of the proposed model is high as specified above when seen in all learning percentages. For now, at 90% learning percentage, the NPV of the recommended combined-MLUDA-NN is 33.3% improved than T-MLUDA-NN, 100% improved than T-DA-NN, and 75% improved than T-PSO-NN that is denoted in Figure 5 (g).

On considering the overall performance from Table 3, the accuracy of the implemented combined-MLUDA-NN method is 3.70% better than T-LM-NN, 12% better than T-PSO-NN, and T-GWO-NN, and 7.69% better than T-DA-NN, and 16.6% better than T-MLUDA-NN. Moreover, the precision of the developed combined-MLUDA-NN system is 6.67% enhanced

Table 2.
Overall performance analysis of proposed blood vessel segmentation using standard and optimized gray-level thresholding

Performance measures	Conventional gray-level thresholding	PSO-based gray-level thresholding (Pedersen and Chipperfield, 2010)	GWO-based gray-level thresholding (Mirjalili et al., 2014)	WOA-based gray-level thresholding (Mirjalili and Lewis, 2016)	DA-based gray-level thresholding (Jafari and Chaleshtari, 2017)	MLU-DA-based gray-level thresholding
Accuracy	0.93685	0.9368	0.93671	0.93671	0.93674	0.93852
Sensitivity	0.45396	0.45259	0.44941	0.44945	0.45101	0.51724
Specificity	0.97926	0.97932	0.9795	0.9795	0.9794	0.97551
Precision	0.65781	0.65772	0.65812	0.65812	0.65781	0.64973
FPR	0.020738	0.020683	0.020501	0.020504	0.020603	0.024487
FNR	0.54604	0.54741	0.55059	0.55055	0.54899	0.48276
NPV	0.97926	0.97932	0.9795	0.9795	0.9794	0.97551
FDR	0.34219	0.34228	0.34188	0.34188	0.34219	0.35027
F_1-Score	0.53719	0.53621	0.5341	0.53413	0.53512	0.57596
MCC	0.51454	0.51368	0.51196	0.51198	0.51277	0.54738
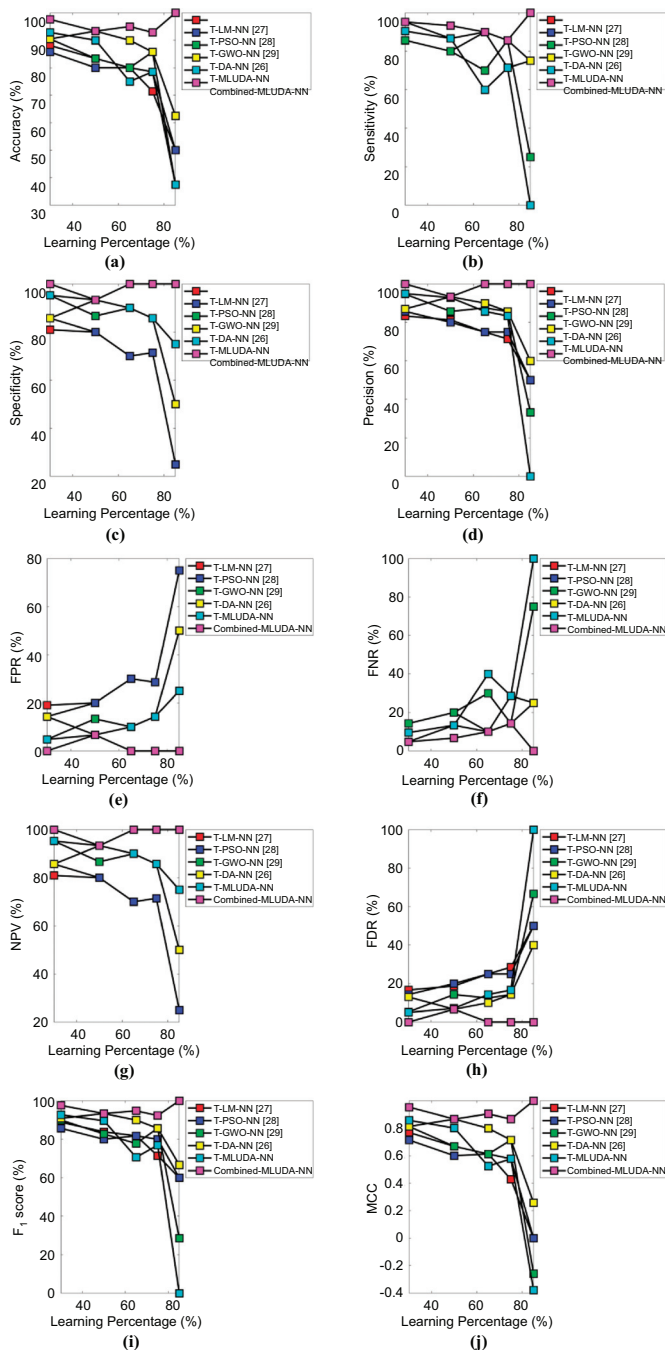
Performance measures	T-LM-NN (Fernández-Navarro et al., 2017)	T-PSO-NN (Pedersen and Chipperfield, 2010)	T-GWO-NN (Mirjalili et al., 2014)	T-DA-NN (Jafari and Chaleshtari, 2017)	T-MLUDA-NN	Combined-MLUDA-NN
Accuracy	0.9	0.83333	0.83333	0.86667	0.8	0.93333
Sensitivity	0.8	0.8	0.8	0.86667	0.8	0.93333
Specificity	1	0.86667	0.86667	0.86667	0.8	0.93333
Precision	1	0.85714	0.85714	0.86667	0.8	0.93333
FPR	0	0.13333	0.13333	0.13333	0.2	0.066667
FNR	0.2	0.2	0.2	0.13333	0.2	0.066667
NPV	1	0.86667	0.86667	0.86667	0.8	0.93333
FDR	0	0.14286	0.14286	0.13333	0.2	0.066667
F_1-Score	0.88889	0.82759	0.82759	0.86667	0.8	0.93333
MCC	0.8165	0.66815	0.66815	0.73333	0.6	0.86667

Table 3.
Overall performance analysis on proposed diabetic retinopathy detection with conventional models

than T-LM-NN, 8.88% enhanced than T-PSO-NN, and T-GWO-NN, 7.69% enhanced than T-DA-NN, and 16.6% enhanced than T-MLUDA-NN. By considering all the measures, the performance of the suggested combined-MLUDA-NN is efficient when compared with other individual texture features. Hence, it can be proved from both a graphical representation and tabular format, that the performance of the proposed combined-MLUDA-NN model is best when compared with other methods.

5.5 Entropy feature analysis
In this context, the performance of the entropy features is compared with the combined-MLUDA-NN model, as shown in Figure 6, and Table 4. Here, the performance of the combined-MLUDA-NN model is compared over the existing E-LM-NN, E-PSO-NN, E-GWO-NN, E-DA-NN and E-MLUDA-NN. In Figure 6 (a), the accuracy of the proposed combined-MLUDA-NN is best for identifying the exact observations at all learning percentages. On considering the learning percentage as 20%, the accuracy of the suggested combined-MLUDA is 2.08% superior to E-DA-NN, 5.37% superior to E-PSO-NN, 8.88% superior to E-GWO-NN, and 11.3% superior to E-MLUDA-NN. Also, the precision of the recommended combined-MLUDA-NN is performing well in recognizing the true positives in the whole learning percentages. It is 21.9% enhanced than E-MLUDA-NN, 28.2% enhanced than E-PSO-NN, and 38.8% enhanced than E-DA-NN at learning percentage 65% based on Figure 6 (d). By evaluating the whole performance from Table 4, the accuracy of the implemented combined-MLUDA-NN is 3.79% better than E-LM-NN and E-GWO-NN, 12% better than E-PSO-NN and E-MLUDA-NN, and 7.69% better than E-DA-NN. Additionally, the specificity of the developed combined-MLUDA-NN system is 6.66% superior to E-LM-NN and E-GWO-NN, 7.69% superior to E-PSO-NN and E-DA-NN, and 16.6% superior to E-MLUDA-NN. Therefore, it is confirmed from Figure 6, and Table 4, that the performance of the proposed combined-MLUDA-NN outperforms other methods with individual feature sets.

5.6 Overall performance analysis variants of NN
Here, the overall performance of the developed MLUDA-NN is evaluated, over other conventionally trained NN. The entire performance is graphically shown in Figure 7 with the variation of learning percentage and the mean performance is tabulated in Table 5. The performance of the implemented MLUDA-NN model is contrasted over LM-NN, PSO-NN,
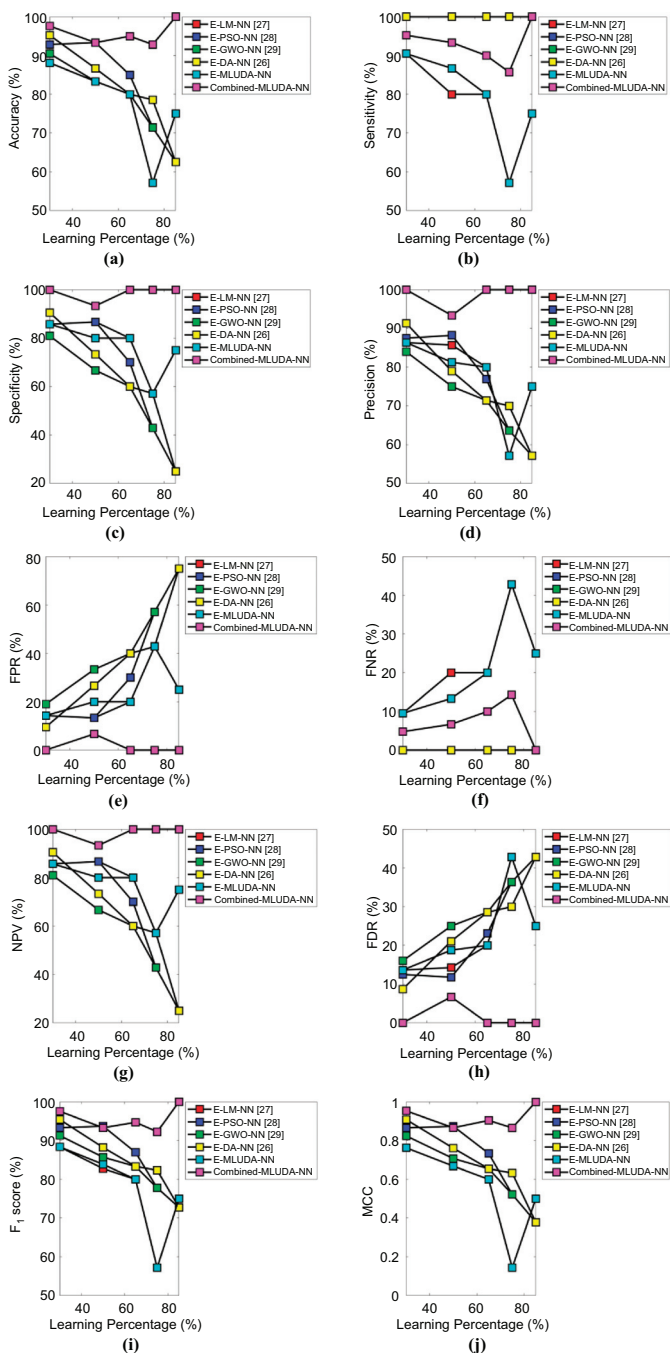
Performance measures	E-LM-NN (Fernández-Navarro *et al.*, 2017)	E-PSO-NN (Pedersen and Chipperfield, 2010)	E-GWO-NN (Mirjalili *et al.*, 2014)	E-DA-NN (Jafari and Chaleshtari, 2017)	E-MLUDA-NN	Combined-MLUDA-NN
Accuracy	0.9	0.83333	0.9	0.86667	0.83333	0.93333
Sensitivity	0.8	0.8	0.8	0.86667	0.86667	0.93333
Specificity	1	0.86667	1	0.86667	0.8	0.93333
Precision	1	0.85714	1	0.86667	0.8125	0.93333
FPR	0	0.13333	0	0.13333	0.2	0.066667
FNR	0.2	0.2	0.2	0.13333	0.13333	0.066667
NPV	1	0.86667	1	0.86667	0.8	0.93333
FDR	0	0.14286	0	0.13333	0.1875	0.066667
F_1-Score	0.88889	0.82759	0.88889	0.86667	0.83871	0.93333
MCC	0.8165	0.66815	0.8165	0.73333	0.66815	0.86667

Table 4.
Overall entropy feature analysis over combined features with optimal trained neural network

GWO-NN and DA-NN. From Figure 7 (a), the accuracy of the suggested MLUDA-NN is recognized in a precise manner overall learning percentages. It is 7.95% better than LM-NN, 11.7% better than DA-NN, and 18.75% better than GWO-NN at learning percentage 50%. The sensitivity of the developed MLUDA-NN model is best in identifying the true negatives at all learning percentages. Now, taking the learning percentage as 85%, the sensitivity of the implemented MLUDA-NN approach is 33.3% better than the GWO-NN and 100% better than the DA-NN as shown in Figure 7 (b). Similarly, the precision of the proposed MLUDA-NN from Figure 7 (d) exhibits the true positives overall learning percentages. At a learning percentage of 30%, the precision of the developed MLUDA-NN method is 5.26% improved than GWO-NN, 11.1% improved than LM-NN, and 17.6% improved than DA-NN. In addition, from Table 5, the overall performance is calculated for the modified MLUDA-NN algorithm with existing algorithms. The accuracy of the proposed MLUDA-NN is 16.6% enhanced than LM-NN, PSO-NN, GWO-NN and DA-NN. Moreover, the specificity of the developed MLUDA-NN is 6.66% superior to LM-NN, 16.6% superior to PSO-NN, GWO-NN, and DA-NN. In addition, NPV of the introduced MLUDA-NN is 27.2% improved than LM-NN, 16.6% improved than PSO-NN, GWO-NN, and DA-NN. Hence, it is verified from the defined outcomes that the implemented MLUDA-NN approach is efficient for DR detection.

5.7 Analysis based on Messidor datasets

The analysis based on Messidor dataset (Decenciere *et al.*, 2014) is shown in Table 6. The accuracy of the proposed MLUDA-NN is 13.04% better than LM-NN, 19.56% better than PSO-NN, 17.39% better than GWO-NN, and 10.86% better than DA-NN. The Sensitivity of the proposed MLUDA-NN is 14.28% advanced than LM-NN, PSO-NN, GWO-NN, and DA-NN. The Specificity of the proposed MLUDA-NN is 12.82% progressed than LM-NN, 20.51% progressed than PSO-NN, 17.94% progressed than GWO-NN, and 10.25% progressed than DA-NN. The Precision of the proposed MLUDA-NN is 38.77% upgraded than LM-NN, 49.58% upgraded than PSO-NN, 46.42% upgraded than GWO-NN, and 34.06% upgraded than DA-NN. The FPR of the proposed MLUDA-NN is 62.50% superior to LM-NN, 72.72% superior to PSO-NN, 70% superior to GWO-NN and 57.14% superior to DA-NN.

5.8 Comparative analysis based on DNN

The analysis based on DNN (Zhang *et al.*, 2019) for two datasets is shown in Tables 7 and 8. Table 7 shows the overall performance analysis of proposed detection with DNN for HRF
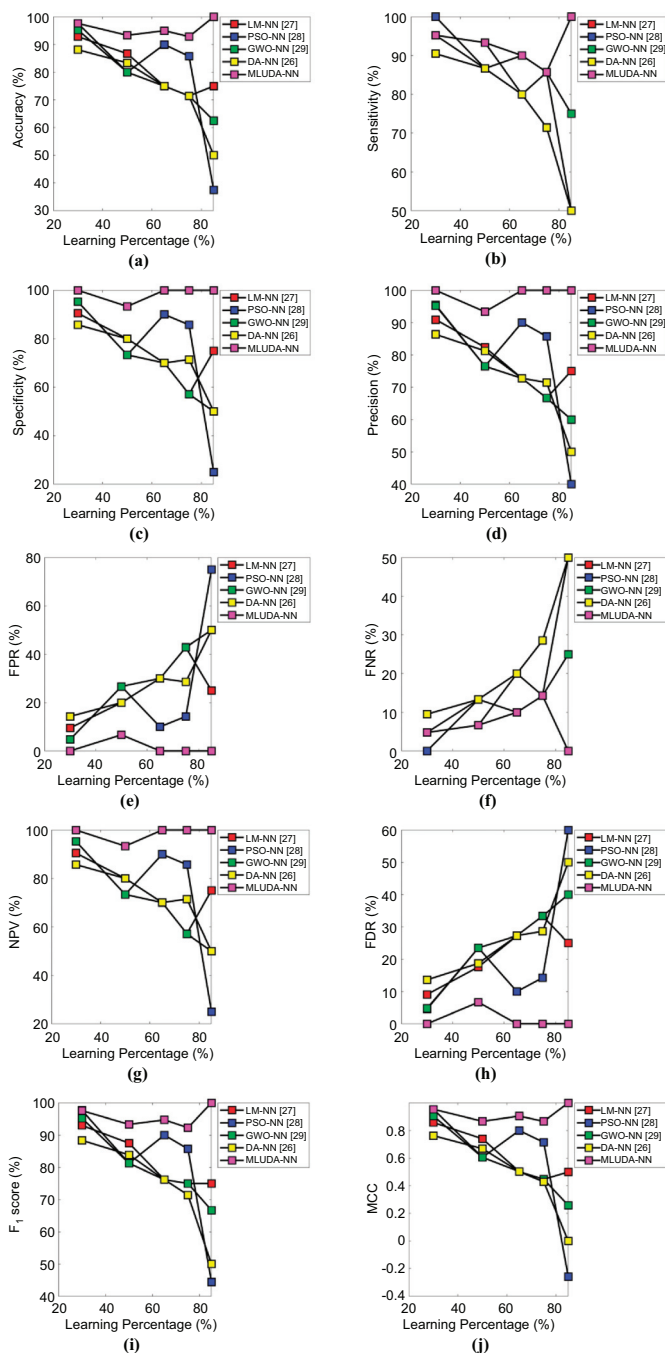
Performance measures	LM-NN (Fernández-Navarro et al., 2017)	PSO-NN (Pedersen and Chipperfield, 2010)	GWO-NN (Mirjalili et al., 2014)	DA-NN (Jafari and Chaleshtari, 2017)	MLUDA-NN
Accuracy	0.8	0.8	0.8	0.8	0.93333
Sensitivity	0.86667	0.8	0.8	0.8	0.93333
Specificity	0.73333	0.8	0.8	0.8	0.93333
Precision	0.76471	0.8	0.8	0.8	0.93333
FPR	0.26667	0.2	0.2	0.2	0.066667
FNR	0.13333	0.2	0.2	0.2	0.066667
NPV	0.73333	0.8	0.8	0.8	0.93333
FDR	0.23529	0.2	0.2	0.2	0.066667
F_1-Score	0.8125	0.8	0.8	0.8	0.93333
MCC	0.60541	0.6	0.6	0.6	0.86667

Table 5.
Overall performance analysis on proposed diabetic retinopathy detection with conventional models

Performance measures	LM-NN (Fernández-Navarro et al., 2017)	PSO-NN (Pedersen and Chipperfield, 2010)	GWO-NN (Mirjalili et al., 2014)	DA-NN (Jafari and Chaleshtari, 2017)	MLUDA-NN
Accuracy	0.8	0.74	0.76	0.82	0.92
Sensitivity	0.75	0.75	0.75	0.75	0.875
Specificity	0.80952	0.7381	0.7619	0.83333	0.92857
Precision	0.42857	0.35294	0.375	0.46154	0.7
FPR	0.19048	0.2619	0.2381	0.16667	0.071429
FNR	0.25	0.25	0.25	0.25	0.125
NPV	0.80952	0.7381	0.7619	0.83333	0.92857
FDR	0.57143	0.64706	0.625	0.53846	0.3
F_1-Score	0.54545	0.48	0.5	0.57143	0.77778
MCC	0.45685	0.37774	0.40231	0.48754	0.73649

Table 6.
Analysis based on Messidor datasets

Performance measures	SVM	NN	DNN	MLU-DA-NN
Accuracy	0.79545	0.86667	0.9	0.93333
Sensitivity	0.59091	0.93333	1	0.93333
Specificity	0.86364	0.8	0.8	0.93333
Precision	0.59091	0.82353	0.83333	0.93333
FPR	0.13636	0.2	0.2	0.066667
FNR	0.40909	0.066667	0	0.066667
NPV	0.86364	0.8	0.8	0.93333
FDR	0.40909	0.17647	0.16667	0.066667
F_1-Score	0.59091	0.875	0.90909	0.93333
MCC	0.45455	0.73994	0.8165	0.86667

Table 7.
Comparative analysis with DNN for HRF datasets

image dataset. From Table 7 the accuracy of the proposed MLU-DA-NN is 17.33% better than SVM, 7.69% better than NN, 3.70% better than DNN. The Sensitivity of the proposed MLU-DA-NN is 57.94% progressed than SVM, 0.001% progressed than NN, and 6.66% progressed than DNN. The FPR of the proposed MLU-DA-NN is 51.10% superior to SVM, 66.66% superior to NN, and DNN. The F_1-Score of the proposed MLU-DA-NN is 57.94%, 6.66%,

Performance measures	SVM	NN	DNN	MLU-DA-NN
Accuracy	0.8	0.8	0.9	0.92
Sensitivity	0.875	0.75	1	0.875
Specificity	0.76471	0.80952	0.88095	0.92857
Precision	0.63636	0.42857	0.61538	0.7
FPR	0.23529	0.19048	0.11905	0.071429
FNR	0.125	0.25	0	0.125
NPV	0.76471	0.80952	0.88095	0.92857
FDR	0.36364	0.57143	0.38462	0.3
F_1-Score	0.73684	0.54545	0.7619	0.77778
MCC	0.60116	0.45685	0.73629	0.73649

Table 8.
Comparative analysis
with DNN for Messidor
datasets

2.66% improved than SVM, NN, and DNN. The MCC of the proposed MLU-DA-NN is 90.66% upgraded than SVM, 17.12% upgraded than NN, and 6.14 upgraded than DNN. Table 8 shows the comparative analysis of Messidor dataset. From Table 8 the specificity of the proposed MLU-DA -NN is 21.42% advanced than SVM, 40.70% advanced than NN, 5.40% advanced than DNN. The precision of the proposed MLU-DA-NN is 10% progressed than SVM, 63.33% progressed than NN, and 13.75% progressed than DNN. The FPR of the proposed MLU-DA-NN is 69.64% superior to SVM, 62.50% superior to NN, and 40% superior to DNN. The NPV of the proposed MLU-DA-NN is 21.42%, 14.70%, 5.40% improved than SVM, NN, and DNN. The F_1-Score of the proposed MLU-DA-NN is 5.55% better than SVM, 42.59% better than NN, and 2.08% better than DNN. The MCC of the proposed MLU-DA-NN is 22.51% upgraded than SVM, 61.21% upgraded than NN, and 0.02% upgraded than DNN.

6. Conclusion
This paper has presented a novel implementation for the early detection of DR diagnosis. It has mainly undergone four phases such as image pre-processing, segmentation, feature extraction and classification. The retinal fundus image was considered as input for pre-processing. Here, the image was enhanced by CLAHE, and average filter. Later, the enhanced image was forwarded for blood vessel segmentation using the optimized gray-level thresholding. In addition, in the feature extraction phase, the features from the blood vessels were extracted by LBP, TEM, and entropy. Further, the gathered features were given to a classifier named NN using an optimized training algorithm. Here, the proposed MLU-DA algorithm was used for generating the optimal level of threshold in the gray-level thresholding and training algorithm in NN. To the next of performance comparison over conventional methods, the overall accuracy of the proposed MLU-DA was 16.6% superior to conventional classifiers, and the precision of the developed MLU-DA was 22% better than LM-NN, 16.6% better than PSO-NN, GWO-NN and DA-NN. Finally, it is concluded that the implemented MLU-DA outperformed state-of-the-art algorithms in detecting DR. Finally, it is concluded that the implemented MLU-DA outperformed state-of-the-art algorithms in detecting DR. Even though the optimally trained NN has been providing effective results in DR diagnosis, the upcoming researchers have mammoth emerging areas like deep learning but with minimal training time, finding best features through optimal feature selection and robust classifiers to attain the highest accuracy. Besides detecting DR through blood vessels analysis, the researchers can focus on other retinal abnormalities like microaneurysms, hemorrhages, hard exudates and cotton wool spots as they are playing fundamental roles in providing initial signs for DR.

References

Aguirre-Ramos, H., Avina-Cervantes, J.G., Cruz-Aceves, I., Ruiz-Pinales, J. and Ledesma, S. (2018), "Blood vessel segmentation in retinal fundus images using Gabor filters, fractional derivatives, and Expectation Maximization", *Applied Mathematics and Computation*, Vol. 339, pp. 568-587.

Akram, M.U., Khalid, S. and Khan, S.A. (2013), "Identification and classification of microaneurysms for early detection of diabetic retinopathy", *Pattern Recognition*, Vol. 46 No. 1, pp. 107-116.

Chakraborty, S., Jana, G.C., Kumari, D. and Swetapadma, A. (2019), "An improved method using supervised learning technique for diabetic retinopathy detection", *International Journal of Information Technology*, pp. 1-5.

Decenciere, E., Zhang, X., Cazuguel, G., Lay, B., Trone, C., Gain, P., Ordonez, R., Massin, P., Erginay, A. and Klein, J.-C. (2014), "Feedback on a publicly distributed image database: the messidor database", *Image Analysis and Stereology*, Vol. 33, p. 3, doi: 10.5566/ias.1155.

Farokhian, F., Yang, C., Demirel, H., Wu, S. and Beheshti, I. (2017), "Automatic parameters selection of Gabor filters with the imperialism competitive algorithm with application to retinal vessel segmentation", *Biocybernetics and Biomedical Engineering*, Vol. 37 No. 1, pp. 246-254.

Faust, O., Acharya, R., Ng, E.Y.-K., Ng, K.-H. and Suri, J.S. (2012), "Algorithms for the automated detection of diabetic retinopathy using digital fundus images: a review", *Journal of Medical Systems*, Vol. 36 No. 1, pp. 145-157.

Fernández-Navarro, F., Carbonero-Ruz, M., Alonso, D.B. and Torres-Jiménez, M. (2017), "Global sensitivity estimates for neural network classifiers", in *IEEE Transactions on Neural Networks and Learning Systems*, Vol. 28 No. 11, pp. 2592-2604.

Galshetwar, G.M., Waghmare, L.M., Gonde, A.B. and Murala, S. (2017), "Edgy salient local binary patterns in inter-plane relationship for image retrieval in Diabetic Retinopathy", *Procedia Computer Science*, Vol. 115, pp. 440-447.

Gupta, R. and Undrill, P.E. (1995), "The use of texture analysis to delineate suspicious masses in mammography", *Physics in Medicine and Biology*, Vol. 40, pp. 835-855.

Hassan, G., El-Bendary, N., Hassanien, A.E., Fahmy, A., Shoeb, A.M. and Snasel, V. (2015), "Retinal blood vessel segmentation approach based on mathematical morphology", *Procedia Computer Science*, Vol. 65, pp. 612-622.

Hemanth, D.J., Deperlioglu, O. and Kose, U. (2019), "An enhanced diabetic retinopathy detection and classification approach using deep convolutional neural network", *Neural Computing and Applications*, pp. 1-15.

Hua, C.-H., Huynh-The, T., Kim, K., Yu, S.-Y., Le-Tien, T., Park, G.H., Bang, J., Khan, W.A., Bae, S.-H. and Lee, S. (2019), "Bimodal learning via trilogy of skip-connection deep networks for diabetic retinopathy risk progression identification", *International Journal of Medical Informatics*, Vol. 132, p. 103926.

Imani, E., Javidi, M. and Pourreza, H.-R. (2015), "Improvement of retinal blood vessel detection using morphological component analysis", *Computer Methods and Programs in Biomedicine*, Vol. 118 No. 3, pp. 263-279.

Jafari, M. and Chaleshtari, M.H.B. (2017), "Using dragonfly algorithm for optimization of orthotropic infinite plates with a quasi-triangular cut-out", *European Journal of Mechanics - A: Solids*, Vol. 66, pp. 1-14.

Kar, S.S. and Maity, P.S. (2016), "Blood vessel extraction and optic disc removal using curvelet transform and kernel fuzzy c-means", *Computers in Biology and Medicine*, Vol. 70, pp. 174-189.

Li, T., Gao, Y., Wang, K., Guo, S., Liu, H. and Kang, H. (2019), "Diagnostic assessment of deep learning algorithms for diabetic retinopathy screening", *Information Sciences*, Vol. 501, pp. 511-522.

Liao, S., Law, M.W.K. and Chung, A.C.S. (2009), "Dominant local binary patterns for texture classification", in *IEEE Transactions on Image Processing*, Vol. 18 No. 5, pp. 1107-1118.

Liu, Y.-P., Li, Z., Xu, C., Li, J. and Liang, R. (2019), "Referable diabetic retinopathy identification from eye fundus images with weighted path for convolutional neural network", *Artificial Intelligence in Medicine*, Vol. 99, p. 101694.

Mirjalili, S. and Lewis, A. (2016), "The whale optimization algorithm", *Advances in Engineering Software*, Vol. 95, pp. 51-67.

Mirjalili, S., Mirjalili, S.M. and Lewis, A. (2014), "Grey wolf optimizer", *Advances in Engineering Software*, Vol. 69, pp. 46-61.

Nazir, T., Irtaza, A., Shabbir, Z., Javed, A., Akram, U. and Mahmood, M.T. (2019), "Diabetic retinopathy detection through novel tetragonal local octa patterns and extreme learning machines", *Artificial Intelligence in Medicine*, Vol. 99, p. 101695.

Niemeijer, M., Abramoff, M.D. and Ginneken, B.V. (2009), "Information fusion for diabetic retinopathy CAD in digital color fundus photographs", in *IEEE Transactions on Medical Imaging*, Vol. 28 No. 5, pp. 775-785.

Panda, R., Puhan, N.B. and Panda, G. (2016), "New Binary Hausdorff Symmetry measure based seeded region growing for retinal vessel segmentation", *Biocybernetics and Biomedical Engineering*, Vol. 36 No. 1, pp. 119-129.

Pedersen, M.E.H. and Chipperfield, A.J. (2010), "Simplifying particle swarm optimization", *Applied Soft Computing*, Vol. 10 No. 2, pp. 618-628.

Quellec, G., Russell, S.R. and Abramoff, M.D. (2011), "Optimal filter framework for automated, instantaneous detection of lesions in retinal images", in *IEEE Transactions on Medical Imaging*, Vol. 30 No. 2, pp. 523-533.

Quellec, G., Charrière, K., Boudi, Y., Cochener, B. and Lamard, M. (2017), "Deep image mining for diabetic retinopathy screening", *Medical Image Analysis*, Vol. 39, pp. 178-193.

Salamat, N., Missen, M.M.S. and Rashid, A. (2019), "Diabetic retinopathy techniques in retinal images: a review", *Artificial Intelligence in Medicine*, Vol. 97, pp. 168-188.

Sangeetha, S.N. and Maheswari, P.U. (2018), "An intelligent model for blood vessel segmentation in diagnosing DR using CNN", *Journal of Medical Systems*, Vol. 42 No. 175, pp. 1-10.

Shanthi, T. and Sabeenian, R.S. (2019), "Modified Alexnet architecture for classification of diabetic retinopathy images", *Computers and Electrical Engineering*, Vol. 76, pp. 56-64.

Sopharak, A., Uyyanonvara, B., Barman, S. and Williamson, T.H. (2008), "Automatic detection of diabetic retinopathy exudates from non-dilated retinal images using mathematical morphology methods", *Computerized Medical Imaging and Graphics*, Vol. 32 No. 8, pp. 720-727.

Sreedharan, N.P.N., Ganesan, B., Raveendran, R., Sarala, P., Dennis, B. and Boothalingam, R. (2018), "Grey Wolf optimisation-based feature selection and classification for facial emotion recognition", *IET Biometrics*, Vol. 7 No. 5, pp. 490-499.

Sun, Y. and Zhang, D. (2019), "Diagnosis and analysis of diabetic retinopathy based on electronic health records", *IEEE Access*, Vol. 7, pp. 86115-86120.

Wan, S., Liang, Y. and Zhang, Y. (2018), "Deep convolutional neural networks for diabetic retinopathy detection by image classification", *Computers and Electrical Engineering*, Vol. 72, pp. 274-282.

Zeng, X., Chen, H., Luo, Y. and Ye, W. (2019), "Automated diabetic retinopathy detection based on binocular siamese-like", *Convolutional Neural Network*, Vol. 7, pp. 30744-30753.

Zhang, W., Zhong, J., Yang, S., Gao, Z., Hu, J., Chen, Y. and Yi, Z. (2019), "Automated identification and grading system of diabetic retinopathy using deep neural networks", *Knowledge-Based Systems*, Vol. 175, pp. 12-25.

Zhou, L., Zhao, Y., Yang, J., Yu, Q. and Xu, X. (2018), "Deep multiple instance learning for automatic detection of diabetic retinopathy in retinal images", *IET Image Processing*, Vol. 12 No. 4, pp. 563-571.

Corresponding author
Ambaji S. Jadhav can be contacted at: asjadhavec@gmail.com